ADVANCED ENERGY MATERIALS
www.advenergymat.de

Direct Observation of Ordered Oxygen Defects on the Atomic Scale in Li_2O_2 for Li-O_2 Batteries

Dongdong Xiao, Shanmu Dong, Jing Guan, Lin Gu, Shanming Li, Nijie Zhao, Chaoqun Shang, Zhenzhong Yang, Hao Zheng, Chun Chen, Ruijuan Xiao, Yong-Sheng Hu, Hong Li, Guanglei Cui,* and Liquan Chen*

Lithium-oxygen (Li-O_2) batteries have received considerable attention recently because of their exceptionally high theoretical gravimetric energy densities compared to the currently available lithium-ion batteries,[1–4] which makes them promising for next-generation electrochemical energy storage. However, many scientific and technical challenges have not been addressed yet, which tremendously hinders their practical application; these include poor rate capability and low round-trip efficiency.[5,6]

Although the detailed mechanisms of oxygen reaction in Li-O_2 batteries have not been well understood, it has been well established that the net reaction is the reduction of oxygen to form Li_2O_2 upon discharge and its subsequent decomposition to release O_2 upon charge.[7–9] Therefore, the formation of Li_2O_2 and its corresponding electronic structure and configuration are expected to significantly influence the discharge and subsequent charge voltage profile, the discharge capacity, and the rate capability. Much effort has been directed toward understanding the growth and structure of Li_2O_2 to improve the performance of Li-O_2 battery.[10–14] It is found that the discharge product Li_2O_2 usually displays a characteristic toroidal-like shape with size up to sub-micrometer when the battery is discharged to high capacity in stable electrolytes (e.g., ethers and dimethylsulfoxide (DMSO)).[15–17] In addition, a LiO_2-like structure was also detected on the surface of Li_2O_2 by magnetic measurements.[12] Such superoxide-like structure likely increases the electronic conductivity of Li_2O_2, which may facilitate charge transport to reduce overpotential during charge process, as suggested by theoretical and experimental research.[18–20] Nonetheless, there remains lack of direct knowledge for the atomic-scale surface structure of electrochemically formed Li_2O_2 particles. In addition, the nature of Li_2O_2 has also been recently proven to be an important factor that affected charge potential. The formation of quasi-amorphous or nanocrystalline Li_2O_2 by controlling the discharge current rate or introducing catalysts can lead to lowered charge potential.[14,21,22] Thus it can be seen that the defective Li_2O_2 may display enhanced transport properties, leading to improved cell performance. However, the look of the structural defects is not clear. Consequently, the lack of detailed microstructure information of the discharge product Li_2O_2, especially at the atomic scale, hinders a fundamental understanding of the mechanism governing the formation and decomposition of Li_2O_2 particle and the role of catalyst during the discharge/charge processes of Li-O_2 batteries.

Here, we carry out a study of the atomic-scale structure of Li_2O_2 by combining annular bright field scanning transmission electron microscopy (ABF-STEM) allowing direct observation of light atoms (e.g., Li, O) at atomic resolution[23,24] with first principle calculations. To the best of our knowledge, this is the first experimental report on the microstructure of discharge product Li_2O_2 at the atomic scale, which may give new insights into the relationship between structure of Li_2O_2 and electrochemical behavior of Li-O_2 batteries.

The porous cathode in this work consists of Super P carbon black being an electronically conductive agent and $NiCo_2O_4$ electrocatalyst. The assembled battery undergoes galvanostatical discharge-charge at 0.04 mA cm^{-2}, and the initial discharge-charge profile is recorded (Figure S1, Supporting Information). The morphological changes of porous cathode before and after discharge were examined using scanning electron microscopy (SEM) and shown in **Figure 1**a,b. It can be clearly seen that after discharge the characteristic toroidal-shaped Li_2O_2 particles with a wide range of diameters are formed on the surface of electrode, which are in agreement with previous work.[12,14–16] Upon closer inspection, it is found that the Li_2O_2 toroids consist of nanocrystalline aggregates, which probably suggest Li_2O_2 grows onto the surface of cathode through superoxide dissolved in solution.[17,25,26] In order to further reveal the details about internal structure of Li_2O_2 particles, aberration-corrected ABF-STEM imaging is applied to directly observe the atomic-scale structure of the discharge product.

Because the Li_2O_2 particles are found to be severely sensitive to electron beam irradiation, and a greatly reduced radiation dose was adopted to minimize beam damage. Note that higher acceleration voltage may induce compromised knock-on damage, which, on the other hand, can minimize the ionization

D. D. Xiao, Prof. L. Gu, S. M. Li, N. J. Zhao, Z. Z. Yang, H. Zheng, Dr. R. J. Xiao, Prof. Y.-S. Hu, Prof. H. Li, Prof. L. Q. Chen
Institute of Physics
Chinese Academy of Sciences/Beijing National Laboratory for Condensed Matter Physics
Beijing 100190, P. R. China
E-mail: l.gu@iphy.ac.cn

Dr. S. M. Dong, Dr. J. Guan, C. Q. Shang, Prof. G. L. Cui
Qingdao Key Lab of Solar Energy Utilization and Energy Storage Technology
Qingdao Institute of Bioenergy and Bioprocess Technology
Chinese Academy of Sciences
Qingdao 266101, P. R. China
E-mail: cuigl@qibebt.ac.cn

C. Chen
Department of Chemistry
Beijing Institute of Technology
Beijing 102488, P. R. China

DOI: 10.1002/aenm.201400664

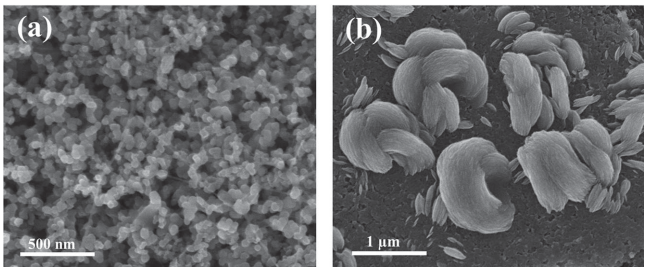

Figure 1. Typical SEM images for a) $NiCo_2O_4$/Super P pristine electrode and b) the toroid-like particles in electrode when discharged to 2.0 V at 0.04 mA cm^{-2}.

damage due to the insulating nature of the reaction products. **Figure 2**a shows the ABF-STEM image of Li_2O_2 taken along the [110] zone axis. In ABF image, the atom columns appear as dark spots due to absorption-type contrast exhibited by ABF imaging, and the contrast demonstrates $Z^{1/3}$ dependence with respect to atomic number, therefore displaying high sensitivity to light atoms.[27] Note that the lithium atomic columns and oxygen-oxygen columns pairs in Li_2O_2 were not resolved to minimize the radiation damage, and the oxygen dimer appears a single dark spot as shown in Figure 2a. However, important details about the atomic-scale structure of Li_2O_2 particles were successfully retained. From Figure 2a, it is obvious that a relative irregular outmost surface layer different from interior was formed on the Li_2O_2 surface. It is reasonable to infer that such defective Li_2O_2 surface may be beneficial for charge transport on the basis of previous work.[18–20] Detailed contrast analyses from the line profile acquired at the box region (shown in Figure 2b) demonstrate an unexpected peroxide vacancy staging phenomenon that the perfect LiO_2 layer and oxygen-deficient LiO_2 layer, which are marked by the green and red arrows in Figure 2a, respectively, occupy every other layer along the *c* axis. And a structure schematic of such staged Li_2O_2 is illustrated in Figure 2c, wherein oxygen atom columns in perfect and defective LiO_2 layers are highlighted by green and red spheres, respectively. Due to the introduction of oxygen defect, the local environment of oxygen in defective LiO_2 layer is different from that in perfect one, leading to distinct oxygen atom columns (e.g., O1 and O2 in Figure 2c). Although the origin of the peroxide vacancy stage ordering in the Li_2O_2 is still mysterious at this phase, the formation of staging structure may be thermodynamically favorable as we discuss later according to the first principle calculation. Meanwhile, it is worth noting that the addition of catalyst has been reported to promote the formation of defective Li_2O_2, contributing to an enhanced oxygen reduction reaction and/or oxygen evolution reaction.[21] This suggests that the $NiCo_2O_4$ catalyst may play an important role in the appearance of staged Li_2O_2. Extended studies should be undertaken to further clarify the formation mechanism and the factor affecting the formation of peroxide vacancy staging, such as discharge rate, catalyst. In addition, from the transport point of view, we expect that such ordered oxygen defect may also provide facile transport path for electron or Li^+ ion through the Li_2O_2 during discharge as other extended defects such as surface,[19] grain boundary,[22] or amorphous layer.[14] Further investigation is needed to understand the effect of ordered oxygen defect on the transport properties of Li_2O_2.

In order to estimate the oxygen deficiency in Li_2O_2, lattice models with different content of oxygen are constructed to simulate the ABF images. We found the simulated ABF image, particularly the contrast of defective LiO_2 layer, shows reasonable agreement with experimental one when the content of peroxide vacancy in defective LiO_2 layer is around 20% (as shown in Figure 2d), compared with those of perfect (Figure 2e) and defective Li_2O_2 with other different content of peroxide vacancy (Supporting Information Figure S2). In addition, electron energy-loss spectroscopy (EELS) was carried out to further investigate electronic structure of the discharge product Li_2O_2 by comparing with commercial Li_2O_2. The Li and O K edge EELS spectra were acquired (**Figure 3**a,b). It is interesting to observe the apparent difference in EELS fine structure between electrochemically formed and commercial Li_2O_2, which indicates the Li and O local structure of discharge

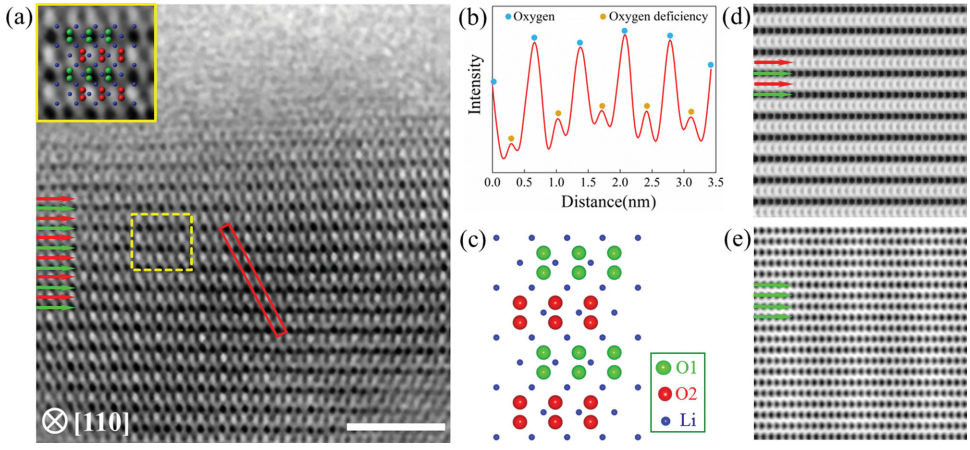

Figure 2. a) ABF-STEM image for Li_2O_2 along the [110] zone axis, the inset at the top left is enlarged image of the selected region; b) the corresponding line profile acquired from the red box region; c) lattice model of defective Li_2O_2, wherein the oxygen atom columns in perfect and defective LiO_2 layer are indicated by green sphere O1 and red sphere O2, respectively; and d,e) simulated ABF images of Li_2O_2 with 20% peroxide vacancy and perfect Li_2O_2, respectively. In the ABF line profile, image contrast of the dark dots is inverted and displayed as peaks. The perfect and oxygen-deficient LiO_2 layers are marked by the green and red arrows, respectively. Scale bar indicates 3 nm.

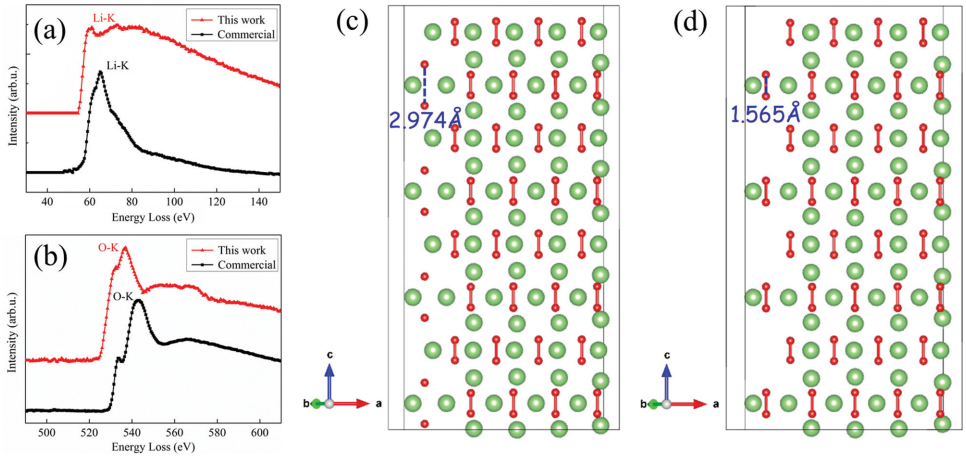

Figure 3. a) Li-K edge and b) O-K edge EELS spectra of electrochemically formed Li_2O_2 in this work and commercial Li_2O_2. The layered structures of c) $Li_{72}O_{72}$ and d) $Li_{68}O_{72}$ with Li vacancies created from $Li_{80}O_{72}$. Lithium and oxygen atoms are labelled with green and red, respectively.

product are not the same as the commercial one. This further confirms that structural defects are introduced during the formation and growth of Li_2O_2, which, moreover, leads to distinct electronic structure closely related to the transport properties. Additionally, the quantitative analysis of EELS spectra indicates the oxygen deficiency is about 15% ± 5%, showing reasonable agreement with result obtained by simulation of ABF image.

Based on these experimental findings, the structure defects of Li_2O_2 with around 20% of peroxide vacancy in the deficient-oxygen LiO_2 layer have been further investigated by first-principle calculation using a supercell with 160 atoms ($Li_{80}O_{80}$) (Supporting Information Figure S3). As one O_2^{2-} group was extracted from every other oxygen layer in $Li_{80}O_{80}$, three distinct arrangements of peroxide vacancy in $Li_{80}O_{72}$ were generated (Supporting Information Figure S4a–c). We found the presence of peroxide vacancy in the defective LiO_2 layer of Li_2O_2 results in cleavage of one of the O-O bonds ($d_{O\text{-}O}$ = 2.983 Å) in the next stack of perfect LiO_2 layer, which is probably due to the requirement to preserve electroneutrality. And the large positive formation energy (E_f = 13.3 eV) of $Li_{80}O_{72}$ revealed that an O-removal reaction to form these structures is not thermodynamically favored. Moreover, the corresponding disordered oxygen arrangement in $Li_{80}O_{72}$ is inconsistent with the simulated ABF images. Therefore, it is likely that the introduction of peroxide vacancy is accompanied by Li removal to minimize the O-O bond-breaking distortion. Two possible structure types of Li vacancies derived from $Li_{80}O_{72}$ are shown in Figure 3c,d. In Figure 3c a pair of Li ions proximate to the two disturbed oxygen atoms was extracted, leading to the intermediate composition of $Li_{72}O_{72}$. Such Li extraction had little effect on restoring the broken O-O bond, as evidenced by the O-O distance of 2.974 Å in $Li_{72}O_{72}$. Subsequently, one Li ion nearby peroxide vacancy is further extracted from the defective LiO_2 layers of $Li_{72}O_{72}$, creating nonstoichiometric $Li_{68}O_{72}$ (Figure 3d). Such Li extraction results in the O-O bond length from 2.974 Å back to 1.565 Å, which is similar with that of $Li_{80}O_{80}$. This strengthened O-O bond can also be manifested by the exothermic energy of –6.2 eV in the process of Li extraction from $Li_{72}O_{72}$ to give the oxygen-rich $Li_{68}O_{72}$. Therefore we conclude that this defective non-stoichiometric structure of $Li_{68}O_{72}$ can explain the main structure feature of the discharge product Li_2O_2 revealed by ABF-STEM imaging. Importantly, the superoxide-like character of discharge product Li_2O_2 is in part accord with previous report.[12,20] This character may facilitate electron transfer and consequently impact reversible formation/decomposition of Li_2O_2. However, this unique staging observed from ABF-STEM is different from the previously reported core-shell structure with oxygen-rich superoxide-like shell layer.

In conclusion, the atomic-scale structure of discharge product Li_2O_2 was successfully revealed using aberration-corrected ABF-STEM imaging. Irregular surface structure and a unique stage ordering in Li_2O_2 that peroxide vacancy preferably occupies every other layer along the *c* axis were observed. The content of peroxide vacancy was estimated to be around 20% by combing ABF image simulation with EELS analysis. First-principle calculation indicated the defective Li_2O_2 was still oxygen-rich although the oxygen deficiency existed. These findings may open up new opportunities to investigate the structure evolution of Li_2O_2 during discharge or charge, hence enable improved understanding of the mechanism of oxygen reaction in Li-O_2 batteries.

Experimental Section

Electrochemical Measurements: The cathodes for Li-O_2 battery were prepared by mixing 40 wt% $NiCo_2O_4$ with 50 wt% Super P and 10 wt% polytetrafluoroethlyene (PTFE) binders. The $NiCo_2O_4$-based cathodes were rolled into slice and cut into squire pieces of 0.5 cm × 0.5 cm (typically 2.0 mg cm^{-2}). More details on the preparation of $NiCo_2O_4$ catalyst and cathode can be found in ref. [28]. The Li-O_2 cell was prepared using a Swagelok design and constructed inside the glove box under argon atmosphere (<1 ppm H_2O and O_2) using a clean lithium metal disk (8 mm diameter) as anode, a glass-fiber and a polypropylene (Celgard 2400) as separator, 1 M LiTFSI in tetra ethylene glycol dimethylether (TEGDME) as electrolyte. The Li-O_2 cell underwent galvanostatic discharge-charge measurements at 0.04 mA cm^{-2}. The capacity was calculated based on the total mass of cathode (electrocatalyst + carbon + binder). After electrochemical measurement, the cell was disassembled in the Ar-filled glove box, and the discharged cathode was washed with dimethyl carbonate (DMC) and dried under vacuum for further analysis.

Characterization: The morphology of discharged cathode was observed on a Hitachi S4800 field emission scanning electron microscope. Aberration-corrected annular-bright-field imaging was performed using a JEOL ARM 200F (JEOL, Tokyo) transmission electron microscope. The attainable resolution defined by the probe forming objective lens was better than 80 picometer. All images were obtained using an illumination semiangle of 25 mrad with the corresponding collection semiangle from 12 to 25 mrad. The raw images were processed with an average background subtraction filter (ABSF) to reduce noise.[29] ABF-STEM image simulation was carried out using the xHREM software (HREM research Inc.). EELS spectra of electrochemically formed Li_2O_2 and commercial one (>90%, Alfa Aesar) were acquired out on a F20 transmission electron microscope (FEI, Eindhoven, The Netherlands) with a Gatan imaging filter (GIF). The relative content of oxygen was evaluated based on quantitative analysis of Li-K edge and O-Kedge EELS spectra using Digital Micrograph software. The physics behind the quantitative analysis was described fully in ref. [30].

Calculation Details: First-principles calculations were performed using the plane wave code VASP,[31] with supplied projector augmented wave (PAW) potentials for core electrons.[32] Total energies were calculated using the Heyd-Scuseria-Ernzerhof (HSE) screened hybrid functional,[33] which has been demonstrated to provide a more accurate treatment of solids, particularly in the study of electron-transfer reactions than standard semilocal DFT functionals. The plane wave energy cutoff of 400 eV and a Γ-centered k-point mesh of $2 \times 2 \times 1$ were set for all computations. All structures were relaxed until the total energies were converged to within 10^{-5} eV/atom. The structure of discharge product Li_2O_2 was calculated using a supercell with 160 atoms based on the primitive unit cell of Li_2O_2.

Supporting Information

Supporting Information is available from the Wiley Online Library or from the author.

Acknowledgments

D.D.X. and S.M.D.contributed equally to this work. The authors acknowledge the financial support from the "973" project (2014CB932300), the funding from the Chinese academy of Science and the NSFC (Grant No. 1117434, 21301185).

Received: April 20, 2014
Revised: June 25, 2014
Published online: September 22, 2014

[1] K. M. Abraham, Z. Jiang, *J. Electrochem. Soc.* **1996**, *143*, 1.
[2] T. Ogasawara, A. Débart, M. Holzapfel, P. Novák, P. G. Bruce, *J. Am. Chem. Soc.* **2006**, *128*, 1390.
[3] G. Giriskumar, B. McCloskey, A. C. Luntz, S. Swanson, W. Wilcke, *J. Phys. Chem. Lett.* **2010**, *1*, 2193.
[4] J. S. Lee, S. T. Kim, R. G. Cao, N. S. Choi, M. L. Liu, K. T. Lee, J. Cho, *Adv. Energy Mater.* **2011**, *1*, 34.
[5] P. G. Bruce, S. A. Freunberger, L. J. Hardwick, J. M. Tarascon, *Nat. Mater.* **2012**, *11*, 19.
[6] Y. C. Lu, B. M. Gallant, D. G. Kwabi, J. R. Harding, R. R. Mitchell, M. S. Whittingham, Y. Shao-Horn, *Energy Environ. Sci.* **2013**, *6*, 750.
[7] C. O. Laoire, S. Mukerjee, E. J. Plichta, M. A. Hendrickson, K. M. Abraham, *J. Electrochem. Soc.* **2009**, *113*, 20127.
[8] Z. Q. Peng, S. A. Freunberger, L. J. Hardwick, Y. H. Chen, V. Giordani, F. Bardé, P. Novák, D. Graham, J. M. Tarascon, P. G. Bruce, *Angew. Chem. Int. Ed.* **2011**, *50*, 6351.
[9] W. Xu, V. V. Viswanathan, D. Y. Wang, S. A. Towne, J. Xiao, Z. M. Nie, D. H. Hu, J.-G. Zhang, *J. Power Source* **2011**, *196*, 3894.
[10] B. M. Gallant, R. R. Mitchell, D. G. Kwabi, J. G. Zhou, L. Zuin, C. V. Thompson, Y, Shao-Horn , *J. Phys. Chem. C* **2012**, *116*, 20800.
[11] R. Wen, M. Hong, H. R. Byon, *J. Am. Chem. Soc.* **2013**, *135*, 10870.
[12] J. B. Yang, D. Y. Zhai, H. H. Wang, K. C. Lau, J. A. Schlueter, P. Du, D. J. Myers, Y. K. Sun, L. A. Curtiss, K. Amine, *Phys. Chem. Chem. Phys.* **2013**, *15*, 3764.
[13] R. R. Mitchell, B. M. Gallant, Y. Shao-Horn, C. V. Thompson, *J. Phys. Chem. Lett.* **2013**, *4*, 1060.
[14] B. D. Adams, C. Radtke, R. Black, M. L. Trudeau, K. Zaghib, L. F. Nazar, *Energy Environ. Sci.* **2013**, *6*, 1772.
[15] R. R. Mitchell, B. M. Gallant, C. V. Thompson, Y. Shao-Horn, *Energy Environ. Sci.* **2011**, *4*, 2952.
[16] D. Xu, Z. L. Wang, J. J. Xu, L. L. Zhang, X. B. Zhang, *Chem. Commun.* **2012**, *48*, 6948.
[17] S. H. Oh, R. Black, E. Pomerantseva, J. H. Lee, L. F. Nazar, *Nat. Chem.* **2012**, *4*, 1004.
[18] J. S. Hummelshøj, J. Blomqvist, S. Datta, T. Vegge, J. Rossmeisl, K. S. Thygesen, A. C. Luntz, K. W. Jacobsen, J. K. Nørskov, *J. Chem. Phys.* **2010**, *132*, 071101.
[19] M. D. Radin, J. F. Rodriguez, F. Tian, D. J. Siegel, *J. Am. Chem. Soc.* **2012**, *134*, 1093.
[20] D. Y. Zhai, H. H. Wang, J. B. Yang, K. C. Lau, K. X. Li, K. Amine, L. A. Curtiss, *J. Am. Chem. Soc.* **2013**, *135*, 15364.
[21] E. Yilmaz, C. Yogi, K. Yamanaka, T. Ohta, H. R. Byon, *Nano Lett.* **2013**, *13*, 4697.
[22] J. Lu, Y. Lei, K. C. Lau, X. Y. Luo, P. Du, J. G. Wen, R. S. Assary, U. Das, D. J. Miller, J. W. Elam, H. M. Albishri, D. A. El-Hady, Y.-K. Sun, L. A. Curtiss, K. Amine, *Nat. Commun.* **2013**, *4*, 2383.
[23] Y. Sun, L. Zhao, H. L. Pan, X. Lu, L. Gu, Y.-S. Hu, H. Li, M. Armand, Y. Ikuhara, L. Q. Chen, X. J. Huang, *Nat. Commun.* **2013**, *4*, 1870.
[24] X. Lu, L. Zhao, X. Q. He, R. J. Xiao, L. Gu, Y.-S. Hu, H. Li, Z. X. Wang, X. F. Duan, L. Q. Chen, J. Maier, Y. Ikuhara, *Adv. Mater.* **2012**, *24*, 3233.
[25] R. Black, S. H. Oh, J. H. Lee, T. Yim, B. Adams, L. F. Nazar, *J. Am. Chem. Soc.* **2012**, *124*, 2902.
[26] J. J. Xu, Z. L. Wang, D. Xu, L. L. Zhang, X. B. Zhang, *Nat. Commun.* **2013**, *4*, 2438.
[27] S. D. Findlay, N. Shibata, H. Sawada, E. Okunishi, Y. Kondo, Y. Ikuhara, *Ultramicroscopy* **2010**, *110*, 903.
[28] L. X. Zhang, S. L. Zhang, K. J. Zhang, G. J. Xu, X. He, S. M. Dong, Z. H. Liu, C. S. Huang, L. Gu, G. L. Cui, *Chem. Commun.* **2013**, *49*, 3540.
[29] R. Kilaas, *J. Microsc.* **1998**, *190*, 45.
[30] R. F. Egerton, *Electron Energy-Loss Spectroscopy in the Electron Microscope*, Plenum, New York **1996**.
[31] G. Kresse, J. Furthmüller, *Phys. Rev. B* **1996**, *54*, 11169.
[32] G. Kresse, D. Joubert, *Phys. Rev. B* **1999**, *59*, 1758.
[33] J. Heyd, G. E. Scuseria, M. Ernzerhof, *J. Chem. Phys.* **2003**, *118*, 8207.